Nanocrystals

Rare-Earth Oxide Nanopolyhedra, Nanoplates, and Nanodisks**

Rui Si, Ya-Wen Zhang, Li-Ping You, and Chun-Hua Yan**

The synthesis of colloidal nanocrystals has attracted rapidly growing interest not only due to their remarkable size- and shape-dependent chemical and physical properties but also because of their self-assembly potential for device applications.[1–7] For the preparation of nanomaterials with desirable properties, it remains a challenge to explore robust pathways and unify principles towards the systematic manipulation of their crystal size and shape in different systems. The thermolysis of various organometallic precursors and treatment in surfactant solutions have been regarded as powerful

[*] R. Si, Prof. Dr. Y.-W. Zhang, Prof. Dr. C.-H. Yan
State Key Laboratory of Rare-Earth Materials
Chemistry and Applications
PKU-HKU Joint Lab for Rare-Earth Materials
and Bioinorganic Chemistry
Peking University
Beijing 100871 (P.R. China)
Fax: (+86) 10-6275-4179
E-mail: ywzhang@pku.edu.cn
yan@pku.edu.cn
Prof. L.-P. You
Electron Microscopy Laboratory
Peking University, Beijing 100871 (P.R. China)

[**] Grants-in-aid from NSFC (nos. 20171003, 20221101, 20490210, and 20423005) and the Founder foundation of PKU are gratefully acknowledged.

Supporting information for this article is available on the WWW under http://www.angewandte.org or from the author.

  DOI: 10.1002/ange.200462573

pathways to synthesize size- and shape-controlled nanoparticles,[1,2,5,7–19,22] nanorods,[2,6,13,14,16,20,21] and nanodisks and nanoplates[14,21–23] of metals,[2,6,8,9,11,13,22] semiconductors,[1,5,14,21] and metal oxides.[7,10,12,15–20,23]

More recently, surface-modified rare-earth compound nanocrystals have drawn more attention due to their unique properties and promising applications in, for example, UV shielding, luminescent displays, optical communication, biochemical probes, and medical diagnostics. For instance, Sato et al. obtained ZnO- and CaO-doped CeO_2 nanoparticles in water at 40 °C that show a significantly reduced catalytic activity in oxidation and excellent UV-absorption capability.[24] Haase et al. have prepared colloidal $CePO_4$:Tb/$LaPO_4$ core-shell nanoparticles in diphenyl ether at 200 °C that display green emission with a high quantum yield of 70 %,[4] and van Veggel et al. have reported the synthesis of redispersible Er^{3+}-, Nd^{3+}-, and Ho^{3+}-doped LaF_3 nanoparticles with modified near-infrared emission.[3]

However, an important family of rare-earth compounds, namely colloidal rare-earth oxide nanocrystals (other than ceria), have rarely been synthesized, possibly due to the difficulty in choosing appropriate precursor complexes.[23,25–27] Therefore, to develop a versatile route towards colloidal rare-earth oxide nanocrystals is of some urgency. We report here a novel and general synthesis of rare-earth oxide nanocrystals by thermolysis of their benzoylacetonate complexes in oleic acid/oleylamine solvents to give, depending upon the nature of the metal cations and the selective adsorption effects of the solvents employed, highly dispersible and crystalline rare-earth oxide nanopolyhedra, nanoplates, and nanodisks. Optical characterization showed that the CeO_2 nanopolyhedra and Eu_2O_3 nanodisks have interesting optical properties.

The crystal structure and morphology of the products synthesized under optimal conditions were determined by powder X-ray diffraction (XRD) and transmission electron microscopy (TEM), respectively (Table 1). All the dry, trivalent rare-earth oxides (Ln_2O_3, Ln = La–Y) have a body-centered cubic (*bcc*) structure (space group: *Ia*3), whereas dry CeO_2 has a face-centered cubic (*fcc*) structure (space group: *Fm*3*m*). Figure 1 shows the XRD patterns of four samples.

Table 1: Crystal structures and morphologies of the as-obtained rare-earth oxides synthesized by thermolysis of $Ln(BA)_3(H_2O)_2$ (Ln = La–Y) or $Ce(BA)_4$ in oleic acid (OA)/oleylamine (OM) at 250–330 °C for 20–60 min.[a]

	OA/OM	*T* [°C]	*t* [min]	Structure	Morphology
La_2O_3	1:7	330	60	*Ia*3	7 nm nanoplate
CeO_2	0	250	20	*Fm*3*m*	2.6 nm nanopolyhedron
Pr_2O_3	3:5	310	60	*Ia*3	20 nm nanoplate
Nd_2O_3	3:5	310	60	*Ia*3	11 nm nanoplate
Sm_2O_3	3:5	310	60	*Ia*3	11 nm nanoplate 26 nm nanodisk
Eu_2O_3	3:5	310	60	*Ia*3	12 nm nanoplate 32 nm nanodisk
Gd_2O_3	3:5	310	60	*Ia*3	30 nm nanodisk
Tb_2O_3	3:5	310	60	*Ia*3	34 nm nanodisk
Er_2O_3	3:5	310	60	*Ia*3	43 nm nanodisk
Y_2O_3	3:5	310	60	*Ia*3	65 nm nanodisk

[a] Determined by powder X-ray diffraction (Rigaku D/MAX-2000, $Cu_{K\alpha}$ radiation) and transmission electron microscopy (Philips Tecnai F30, 300 kV).

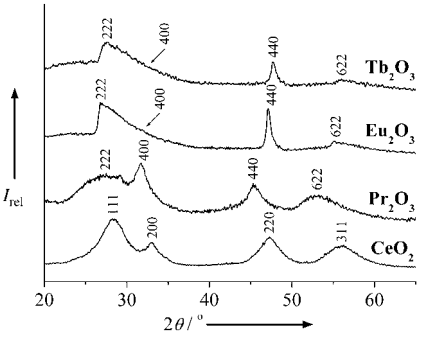

Figure 1. XRD patterns of dry CeO_2, Pr_2O_3, Eu_2O_3, and Tb_2O_3. The calculated lattice constant *a* is 5.4516(3), 11.36(1), 10.97(1), and 10.90(1) Å for CeO_2 (JCPDS: 34-0394), Pr_2O_3,[28] Eu_2O_3 (JCPDS: 34-0392), and Tb_2O_3 (JCPDS: 23-1418), respectively.

The TEM image shown in Figure 2a reveals that the as-obtained CeO_2 nanopolyhedra have a uniform size of 2.6 nm and form a two-dimensional (2D) superlattice structure on the copper grids. The HRTEM image (inset in Figure 2a) shows that each CeO_2 nanopolyhedron is a truncated octahedron enclosed by the (111) and (200) planes.[29]

Figure 2b is the TEM image of the as-obtained Eu_2O_3 redissolved in cyclohexane. Nanodisks with a diameter of about 32 nm have formed, and some of them assemble through their round surface to produce rail-like nanoarrays (see also the Supporting Information). Each slightly flexural Eu_2O_3 nanodisk comprises six (222) layers and has a thickness of 1.6 nm according to the HRTEM image of the side-surface (inset in Figure 2b). The ($\bar{4}40$) planes are perpendicular to (222), and thus the preferential growth direction of the nanodisks is [110]. Each as-obtained Eu_2O_3 nanodisk has a 2D growth structure that is confined along the [111] direction. Figure 2c displays the 2D Eu_2O_3 nanoarrays in a large area. The array axis is [111] and the distance between two adjacent nanodisks is 2.3 nm. Figure 2d shows the TEM image of the Eu_2O_3 nanocrystals redissolved in toluene/hexane (1:1); square nanoplates with a side-size of about 12 nm have formed (see also the Supporting Information). Figure 2e shows that the surface of a nanoplate is composed of the (400) and (040) planes. Each Eu_2O_3 nanoplate is constructed from four (004) layers and has a thickness of 1.0 nm, as determined from the HRTEM image of its side-surface (bottom inset in Figure 2e). The angle between the (222) and (004) planes is close to 60°, which is consistent with the calculated value. The as-obtained Eu_2O_3 nanoplate has a 2D growth structure that is confined along the [001] direction due to symmetry breaking, similar to the case of Gd_2O_3 square nanoplates.[23]

Figures 2f and g show the TEM images of the as-obtained Er_2O_3 and Pr_2O_3, respectively. Pure nanodisks with a diameter of 43 nm are present for Er_2O_3, while pure square nanoplates with a side-size of 20 nm have formed for Pr_2O_3. Figure 2h shows the 2D Pr_2O_3 nanoarrays produced on the copper grids. The array axis is [001] and the distance between two adjacent nanodisks is 2.9 nm.

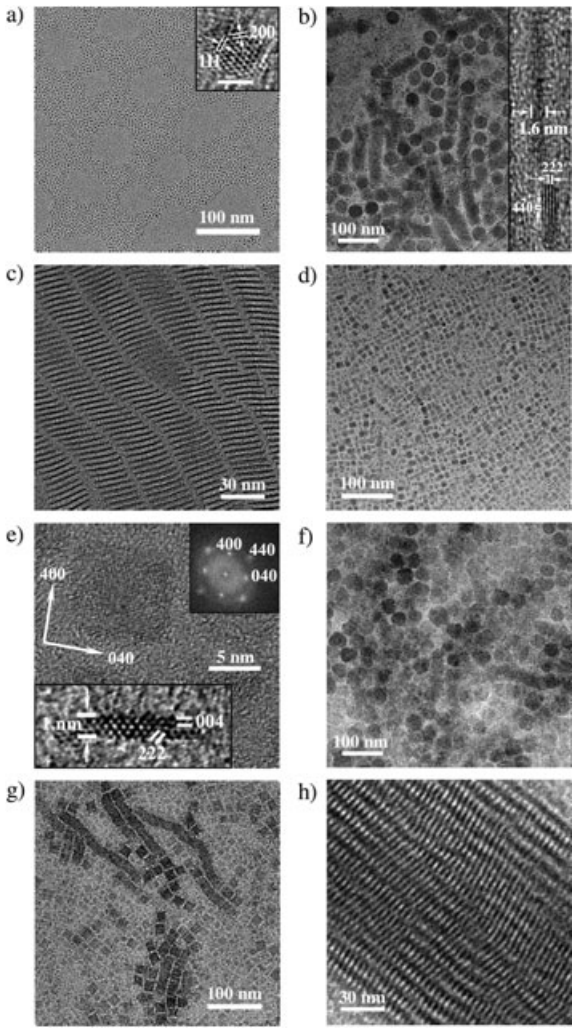

Figure 2. a) TEM image of the as-obtained CeO_2; the inset shows the HRTEM image of a CeO_2 nanopolyhedron (scale bar: 2 nm); b) TEM image of the as-obtained Eu_2O_3 redissolved in cyclohexane; the inset shows the side-surface HRTEM image of a nanodisk; c) TEM image of the 2D Eu_2O_3 nanoarrays; d) TEM image of the as-obtained Eu_2O_3 redissolved in toluene/hexane (1:1); e) The surface and side-surface HRTEM images of an Eu_2O_3 nanoplate; the inset shows the fast Fourier transformation of the surface HRTEM image; f) TEM image of the as-obtained Er_2O_3; g) TEM image of the as-obtained Pr_2O_3; h) TEM image of the 2D Pr_2O_3 nanoarrays.

The mechanism of shape-controlled synthesis of nanocrystals is currently being investigated intensively.[6,12–14,16,17,20–22] During the thermolysis of the precursor complexes the capping ligand (variety, concentration, and selective adsorption onto particular crystallographic facets) plays a critical role in the shape-control process. In our case, experiments show that oleic acid binds more strongly than oleylamine to the surface atoms of the nanocrystals, due to its higher oxophilicity. Increasing the amount of oleic acid gradually dissolved the CeO_2 and greatly improved the solubility of the Ln_2O_3 products in nonpolar solvents. Capping ligands also have distinct effects on the shape of the products formed during the crystal-growth process (Figure 3a).

The thermolysis of rare-earth benzoylacetonate complexes releases a large number of rare-earth oxide nuclei in which the oxygen comes from the chelating ligand.[5] In the *fcc* CeO_2 crystals, the density of surface atoms follows the order $\{111\} > \{100\} > \{110\}$. Generally, the face with a higher density of surface atoms is blocked by the adsorption of surfactants during the crystal growth of colloidal nanocrystals, and the growth along this facet is therefore considerably restricted. However, since oleylamine is characterized by its nonselective adsorption on these faces, the CeO_2 nuclei grow in a 3D mode to generate nanopolyhedra enclosed by both the (111) and (200) planes. The *bcc* structure of Ln_2O_3 can be derived from the *fcc* structure of CeO_2 by removing one-fourth of the oxygen atoms from specific lattice sites. The surface density of atoms in the facets of this structure follows the order $\{100\} > \{111\} > \{110\}$. The former two denser facets are selectively capped by oleic acid, which means that the nuclei grow in a 2D mode to produce nanoplates with confined (001) planes or nanodisks with confined (111) planes. The confinement effect of oleic acid on the specific facets in this case can be demonstrated in the synthesis of Eu_2O_3 nanodisks: decreasing the amount of oleic acid (OA/OM = 1:7) led to some of the Eu_2O_3 nanoparticles showing 3D growth (see Figure 3b). The shape evolution from square nanoplate (La_2O_3–Eu_2O_3) to nanodisk (Sm_2O_3–Y_2O_3) is possibly caused by the change of relative growth rate along {100} to {111} across the Ln_2O_3 series.

Further experiments showed that the size of our rare-earth oxide nanocrystals can be tuned by changing the synthetic parameters, such as the reaction time and temperature. For Eu_2O_3, for example, shortening the reaction time

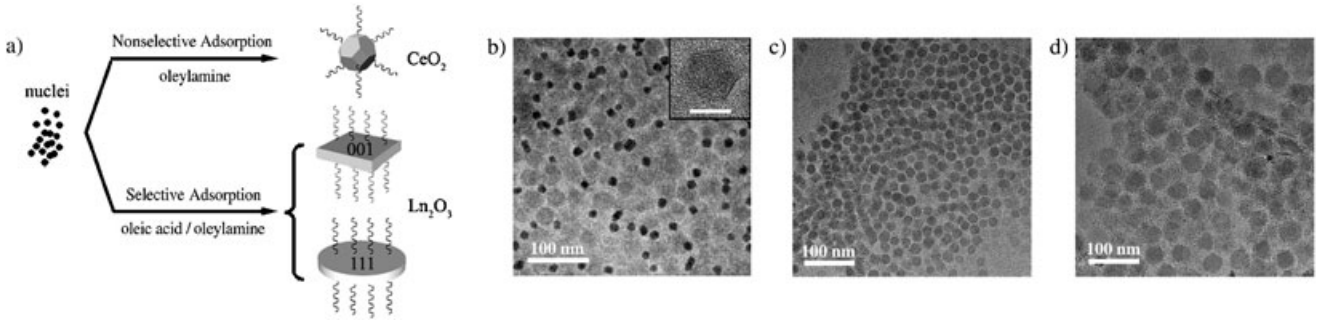

Figure 3. a) Formation of rare-earth oxide nanopolyhedra, nanoplates, and nanodisks. b)–d) TEM images of the as-obtained Eu_2O_3: b) OA/OM = 1:7, 310 °C, 1 h (inset: HRTEM image of an Eu_2O_3 nanoparticle; scale bar: 10 nm); c) OA/OM = 3:5, 310 °C, 20 min; d) OA/OM = 3:5, 330 °C, 1 h.

from 1 h to 20 min caused a decrease in the diameter of the nanodisks from 32 to 20 nm at a reaction temperature of 310 °C (Figure 3c). Upon increasing the reaction temperature from 310 to 330 °C, the size of the nanodisks increased from 32 to 41 nm with a reaction time of 1 h (Figure 3d).

Figure 4a shows the UV/Vis absorption spectrum of the colloidal CeO_2 nanopolyhedra. The spectrum exhibits a strong absorption band at about 300 nm due to the charge-transfer transition from the O 2p to the Ce 4f orbital in CeO_2. Its absorption edge is blue-shifted compared to that of the aggregated CeO_2 nanocrystals in our previous work.[30] Furthermore, the direct bandgap energy, E_d,[31] of the dispersible CeO_2 is 3.60 eV, much larger than that of the aggregated one (3.42 eV). As both CeO_2 samples have the same cubic structure and particle size (2.6 nm), the blue shift of the UV absorption observed for the present monodisperse CeO_2 nanopolyhedra must be related to a modification of the surface state by surface passivation arising from the capping oleylamine ligands.[30]

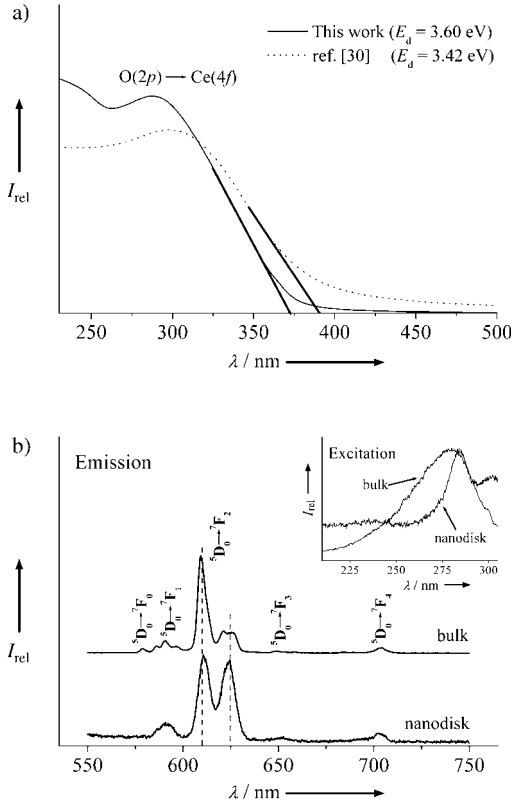

Figure 4. a) UV/Vis absorption spectra (Hitachi U-3010) of the monodisperse CeO_2 nanopolyhedra (solid line) obtained in this work and the aggregated CeO_2 ones of ref. [30] (dotted line). b) Room-temperature fluorescence emission spectra (Hitachi F-4500) of the Eu_2O_3 nanodisks and commercial Eu_2O_3 powders (λ_{ex} = 285 nm); the inset shows their excitation spectra (λ_{em} = 610 nm).

Figure 4b shows the room-temperature emission spectra of Eu_2O_3 nanodisks redissolved in cyclohexane and commercial Eu_2O_3 (99.99 %) powder after excitation at a wavelength of 285 nm. The spectra are described by the $^5D_0 \rightarrow {}^7F_j$ line emissions (J = 0, 1, 2, 3, and 4) of the Eu^{3+} ion.[32] An interesting feature is that the intensity ratio of the peak at 625 nm to the peak at 610 nm is greatly enhanced in the emission spectrum of the Eu_2O_3 nanodisks compared with that of the cubic Eu_2O_3 powders. The emission spectrum of the cubic Eu_2O_3 nanodisks is very similar to that of the monoclinic Eu_2O_3 polycrystalline powders, in which the Eu^{3+} ion occupies a site of lower symmetry.[33] It is known that surface atoms, which have a lower coordination number, usually have lower symmetry than bulk ones. In the present Eu_2O_3 nanodisks, two out of six (222) planes are surface ones and thus the surface fraction of Eu^{3+} ions is very high ($> 1/3$). Therefore, this unusual spectrum is considered to result from the higher fraction of surface Eu^{3+} ions, which occupy a different symmetric site due to their lower coordination number than that of the bulk atoms in the Eu_2O_3 nanodisks.

In summary, we have demonstrated a general synthesis of dispersible rare-earth oxide nanocrystals by thermolysis of their benzoylacetonate complexes in oleic acid/oleylamine, which may represent a general route to nanocrystals of other metal oxides. Due to the selective adsorption of the capping ligands on certain cubic faces during crystal growth, nanocrystals with different morphologies, such as nanopolyhedra, nanoplates, and nanodisks, are created, which exhibit a striking ability to self-assemble into large-area nanoarrays. These novel nanometric architectures with unusual optical properties that result from surface-modification effects are expected to enrich the field of lanthanide chemistry, benefit the development of a shape-control theory for nanocrystals, and promise the fabrication of advanced rare-earth functional materials with new applications.

Experimental Section

Oleylamine (OM, Acros), oleic acid (OA, Alfa), and 1-benzoylacetone (HBA, Acros) were used as received.

Rare-earth complexes: La_2O_3, $Ce_2(CO_3)_3$, Pr_6O_{11}, Nd_2O_3, Sm_2O_3, Eu_2O_3, Gd_2O_3, Tb_4O_7, Er_2O_3, or Y_2O_3 (metal content 6 mmol) was dissolved in 40 mL of deionized water by adding HNO_3. HBA (24 mmol) was dissolved in 80 mL of ethanol by adding $NH_3{\cdot}H_2O$. The above two solutions were mixed together whilst stirring and dilute aqueous NH_3 was then added dropwise (final pH: 6–7). The solution was aged at room temperature for 12 h and then filtered. The precipitate was collected, washed with deionized water, and then dried in vacuo at 40 °C overnight. The yields of the complexes were 40–60 %.

Dispersible rare-earth oxides: To obtain Ln_2O_3 (Ln = La, Pr, Nd, Sm, Eu, Gd, Tb, Er, or Y), $Ln(BA)_3(H_2O)_2$ (0.2 mmol) was added to 15 mL of OA/OM (Table 1) in a three-necked flask at room temperature. Ar was bubbled through the solution for 20 min and then the solvents were removed under vacuum at about 100 °C for 30 min. The flask was then heated to 310–330 °C at a heating rate of 20 K min^{-1} with vigorous magnetic stirring in a temperature-controlled electromantle, and was maintained at this temperature for 1 h under Ar. To obtain CeO_2, $Ce(BA)_4$ (0.5 mmol in 1 mL of OM) was injected into 15 mL of OM at 250 °C and heated for 20 min under Ar. When the reaction was complete, an excess amount of ethanol was poured into the solution at about 70 °C. The resultant mixture was centrifugally separated and the products were collected. The as-precipitated nanocrystals were washed several times with ethanol and then dried in vacuo at 70 °C overnight. The yield of nanocrystals obtained was

about 75%. The as-precipitated nanocrystals could be redissolved in nonpolar solvents such as hexane, toluene, and cyclohexane.

Received: November 10, 2004
Revised: March 3, 2005
Published online: April 21, 2005

Keywords: crystal growth · fluorescence · nanostructures · rare-earth oxides · UV/Vis spectroscopy

[1] C. B. Murray, D. J. Norris, M. G. Bawendi, *J. Am. Chem. Soc.* **1993**, *115*, 8706.
[2] S.-J. Park, S. Kim, S. Lee, Z. G. Khim, K. Char, T. Hyeon, *J. Am. Chem. Soc.* **2000**, *122*, 8581.
[3] J. W. Stouwdam, F. C. J. M. van Veggel, *Nano Lett.* **2002**, *2*, 733.
[4] K. Kömpe, H. Borchert, J. Storz, A. Lobo, S. Adam, T. Möller, M. Haase, *Angew. Chem.* **2003**, *115*, 5672; *Angew. Chem. Int. Ed.* **2003**, *42*, 5513.
[5] W. S. Seo, H. H. Jo, K. Lee, J. T. Park, *Adv. Mater.* **2003**, *15*, 795.
[6] F. Dumestre, B. Chaudret, C. Amiens, M.-C. Fromen, M.-J. Casanove, P. Renaud, P. Zurcher, *Angew. Chem.* **2002**, *114*, 4462; *Angew. Chem. Int. Ed.* **2002**, *41*, 4286.
[7] T. Hyeon, S. S. Lee, J. Park, Y. Chung, H. B. Na, *J. Am. Chem. Soc.* **2001**, *123*, 12798.
[8] D. P. Dinega, M. G. Bawendi, *Angew. Chem.* **1999**, *111*, 1906; *Angew. Chem. Int. Ed.* **1999**, *38*, 1788.
[9] E. V. Shevchenko, D. V. Talapin, H. Schnablegger, A. Kornowski, O. Festin, P. Svedlindh, M. Haase, H. Weller, *J. Am. Chem. Soc.* **2003**, *125*, 9090.
[10] M. Yin, S. O'Brien, *J. Am. Chem. Soc.* **2003**, *125*, 10180.
[11] N. R. Jana, X. Peng, *J. Am. Chem. Soc.* **2003**, *125*, 14280.
[12] J. Cheon, N.-J. Kang, S.-M. Lee, J.-H. Lee, J.-H. Yoon, S. J. Oh, *J. Am. Chem. Soc.* **2004**, *126*, 1950.
[13] V. F. Puntes, K. M. Krishnan, A. P. Alivisatos, *Science* **2001**, *291*, 2115.
[14] M. Monge, M. L. Kahn, A. Maisonnat, B. Chaudret, *Angew. Chem.* **2003**, *115*, 5479; *Angew. Chem. Int. Ed.* **2003**, *42*, 5321.
[15] W. S. Seo, H. H. Jo, K. Lee, B. Kim, S. J. Oh, J. T. Park, *Angew. Chem.* **2004**, *116*, 1135; *Angew. Chem. Int. Ed.* **2004**, *43*, 1115.
[16] N. R. Jana, Y. Chen, X. Peng, *Chem. Mater.* **2004**, *16*, 3931.
[17] H. Zeng, P. M. Rice, S. X. Wang, S. Sun, *J. Am. Chem. Soc.* **2004**, *126*, 11458.
[18] F. X. Redl, C. T. Black, G. C. Papaefthymiou, R. L. Sandstrom, M. Yin, H. Zeng, C. B. Murray, S. P. O'Brien, *J. Am. Chem. Soc.* **2004**, *126*, 14583.
[19] J. Park, K. An, Y. Hwang, J.-G. Park, H.-J. Noh, J.-Y. Kim, J.-H. Park, N.-M. Hwang, T. Hyeon, *Nat. Mater.* **2004**, *3*, 891.
[20] P. D. Cozzoli, A. Kornowski, H. Weller, *J. Am. Chem. Soc.* **2003**, *125*, 14539.
[21] A. Ghezelbash, M. B. Sigman, Jr., B. A. Korgel, *Nano Lett.* **2004**, *4*, 537.
[22] V. F. Puntes, D. Zanchet, C. K. Erdonmez, A. P. Alivisatos, *J. Am. Chem. Soc.* **2002**, *124*, 12874.
[23] Y. C. Cao, *J. Am. Chem. Soc.* **2004**, *126*, 7456.
[24] R. Li, S. Yabe, M. Yamashita, S. Momose, S. Yoshida, S. Yin, T. Sato, *Solid State Ionics* **2002**, *151*, 235.
[25] W. P. Hsu, L. Rönnquist, E. Matijević, *Langmuir* **1988**, *4*, 31.
[26] M. Yada, M. Mihara, S. Mouri, M. Kuroki, T. Kijima, *Adv. Mater.* **2002**, *14*, 309.
[27] X. Wang, X. M. Sun, D. P. Yu, B. S. Zou, Y. D. Li, *Adv. Mater.* **2003**, *15*, 1442.
[28] G. V. Samsonov, *The Oxide Handbook*, 2nd ed., IFI/Plenum, New York, **1982**, p. 13.
[29] Z. L. Wang, X. Feng, *J. Phys. Chem. B* **2003**, *107*, 13563.
[30] Y. W. Zhang, R. Si, C. S. Liao, C. H. Yan, C. X. Xiao, Y. Kou, *J. Phys. Chem. B* **2003**, *107*, 10159.
[31] R. A. Van Leeuwen, C.-J. Hung, D. R. Kammler, J. A. Switzer, *J. Phys. Chem.* **1995**, *99*, 15247.
[32] G. Blasse, B. C. Grabmaier, *Luminescent Materials*, Springer, Berlin, **1994**.
[33] K. C. Sheng, G. M. Korenowski, *J. Phys. Chem.* **1988**, *92*, 50.

